Kinetic study on degradation of tylosin in aqueous media using potassium peroxydisulfate in the presence of immobilized nanosilver

S. Kamali Moghaddam, M.H. Rasoulifard*, M. Vahedpour, M.R. Eskandarian

Department of Chemistry, University of Zanjan, Zanjan, Iran, Tel. +98 24 33052591; Fax: +98 24 33052477;
emails: kamali8963@yahoo.com (S. Kamali Moghaddam), m_h_rasoulifard@znu.ac.ir (M.H. Rasoulifard), Tel. +98 24 33052631;
Fax: +98 24 33052477; email: vahed@znu.ac.ir (M. Vahedpour), Tel. +98 91 23415643; Fax: +98 24 33052477;
email: m.r.eskandarian@gmail.com (M.R. Eskandarian)

ABSTRACT

In the present research, the degradation of tylosin (TYL) by nano $Ag/S_2O_8^{2-}$ process under various reaction conditions was investigated. The experiments were performed in a batch reactor, using nanosilver as a catalyst. Effects of pH, persulfate concentration, temperature, and catalytic nano Ag on the degradation efficiency of TYL by persulfate are examined. For treatment of solutions containing 50 mg/L of TYL, the optimum obtained conditions were: 0.4 g/L of nano Ag, 100 mM of the KPS, initial pH of 6.0, and temperature of 40°C. The degradation of TYL by nano $Ag/S_2O_8^{2-}$ oxidation process has been found to follow the pseudo-first-order kinetic model. Finally rate equation for TYL degradation using Langmuir–Hinshelwood kinetic model is:

$$r = 9630.5 \exp\left[-\frac{32.552}{RT}\right] C^{0.9925}$$

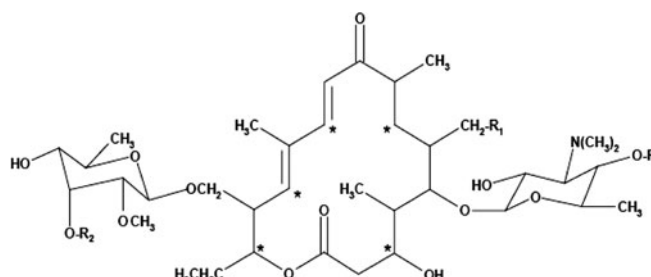*Keywords:* Advanced oxidation processes (AOPs); Kinetics; Tylosin; Nanosilver; Peroxydisulfate

1. Introduction

Largely used in livestock, veterinary pharmaceutically active compounds are now identified as environmental issue. Public concern on their environmental fate and occurrence increased in recent years [1]. Until recently, antibiotics have received comparatively little attention as pollutants in the aquatic environment which is surprising considering that unlike many other pollutants, antibiotics have a direct biological action on microbes [2]. From an environmental engineering point of view, pharmaceuticals including antibiotics are a new group of man-made chemicals of concern entering the environment at concentrations such that the health effects are unknown [3]. Among veterinary pharmaceuticals, tylosin (TYL) is a 16-membered ring microcline antibiotic (molecular formula = $C_{46}H_{77}NO_{17}$, molecular weight = 916.12) (Table 1), produced by fermentation of Streptomycin strains [4]. TYL has been used worldwide in a variety of food animal species to prevent and treat respiratory, enteric, and other diseases. It has also been used to enhance the efficiency of food utilization. TYL may enter the environment through its use in animals [5].

*Corresponding author.
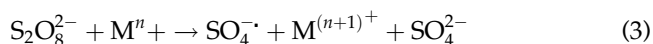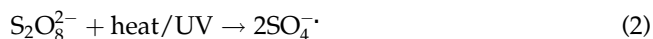
Table 1
Chemical structure and properties of tylosin

Name	Tylosin
Structure	
Molecular formula	$C_{46}H_{77}NO_{17}$
λ_{max} (nm)	300
Molecular weight (g/mol)	916.12

Antibiotics are hazardous contaminants in the aquatic environment because of their adverse effects on aquatic life and humans [3]. Thus, the search for new alternatives to prevent water contamination is necessary, considering the risks that residual pharmaceuticals can present to human health and to the environment. The advanced oxidation processes (AOPs) are considered as good alternatives due to their high efficiency in oxidizing a great variety of organic compounds. Most AOPs are based on the generation of HO· radicals in the medium, which follow from traditional methods to newly scrutinized biological modus operandi HO· (E^0 = 2.720 V vs. NHE) [6–10]. Key AOPs include heterogeneous and homogeneous photocatalysis based on near ultraviolet (UV) or solar visible irradiation, electrolysis, ozonation, the Fenton's reagent, ultrasound, and wet air oxidation, while less conventional but evolving processes include ionizing radiation, microwaves, pulsed plasma, and the ferrate reagent [11–15]. AOPs although making use of different reacting systems, are all characterized by the same chemical feature: production of OH radicals. OH radicals are extraordinarily reactive species; they attack the most part of organic molecules with rate constants usually in the order of 10^6–10^9 $M^{-1} s^{-1}$. They are also characterized by a little selectivity of attack, which is a useful attribute for an oxidant used in wastewater treatment and for solving pollution problems [16]. Persulfate ($S_2O_8^{2-}$) is the newest oxidant used in *in situ* chemical oxidation for groundwater and soil cleanup. $S_2O_8^{2-}$ itself is a strong oxidant with a standard oxidation potential (E^0) of 2.01 V (Eq. (1)) [17].

$$S_2O_8^{2-} + 2e \rightarrow 2SO_4^{2-} \tag{1}$$

Heat, transition metal ions (M^{n+}), and UV light can excite $S_2O_8^{2-}$ to form a sulfate radical ($SO_4^{-\cdot}$), a stronger oxidant (E^0 = 2.60 V) than $S_2O_8^{2-}$, to significantly enhance the oxidation of contaminants, as shown in the following equations [18]:

$$S_2O_8^{2-} + heat/UV \rightarrow 2SO_4^{-\cdot} \tag{2}$$

$$S_2O_8^{2-} + M^{n}+ \rightarrow SO_4^{-\cdot} + M^{(n+1)^+} + SO_4^{2-} \tag{3}$$

Hydroxyl radicals can also be formed via Eqs. (4) and (5) in the peroxydisulfate-water system. Both ($SO_4^{-\cdot}$) and HO· are possibly responsible for the destruction of organic contaminants [18].

$$SO_4^{-\cdot} + H_2O \rightarrow HO^{\cdot} + H^+ + SO_4^{2-} \tag{4}$$

$$SO_4^{-\cdot} + HO^- \rightarrow SO_4^{2-} + HO^{\cdot} \tag{5}$$
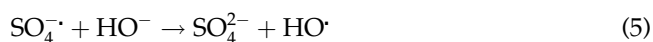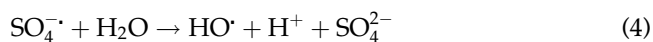
Application of nano Ag-catalyzed peroxydisulfate, as an advanced oxidation process, introduces an effectual method for water and wastewater treatment. An accelerated reaction using $S_2O_8^{-2}$ to destroy antibiotics can be achieved via chemical activation with nanosilver to generate sulfate radicals ($SO_4^{-\cdot}$).

2. Experimental

2.1. Materials and methods

All reagents used in the present study were of analytical reagent grade and used without any further purification. Tyloject 20% (TYL) was provided from Razak (Iran). The content of basic TYL was 80.0% from TYL A, and the sum of the contents of TYL A, TYL B, TYL C, and TYL D was not less than 95.0%. Immobilized silver nanoparticles were purchased from Tehran Shimi Co. and potassium peroxydisulfate from
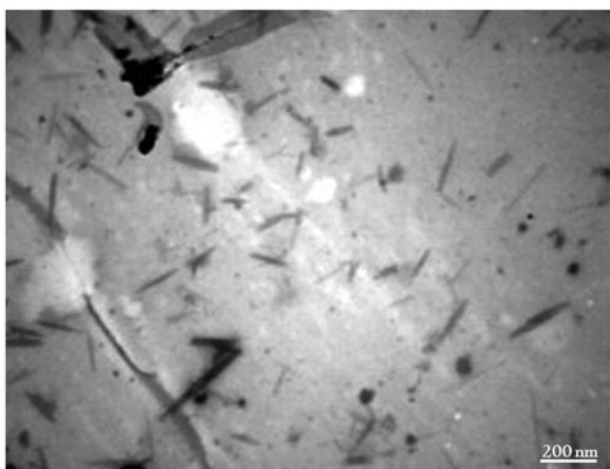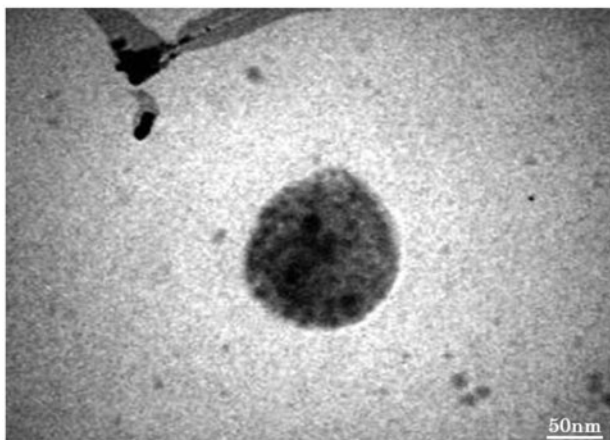
Fig. 1. SEM image of the Ag nanoparticles.

Fig. 2. TEM image of the Ag nanoparticles.

Merck. Experiments were carried out in a batch reactor during 35 min. The required amounts of TYL from stock solution and $S_2O_8^{2-}$ were poured into the glass bottle and then diluted with distilled water to 100 mL. The reaction was initiated by adding different amounts of nano Ag to the reactor. Scanning electron microscopy (SEM) images were obtained by TESCAN VEGAN II LMH (Czech Republic). Transmission electron microscopy (TEM) image was obtained using a (TEM 906, Leo, Germany). Figs. 1 and 2 represent the SEM and TEM images of the nano Ag particles which are utilized in present research, respectively. In addition, mean size of the nano Ag particles was 50–60 nm accordingly.

The start time was recorded in order to measure the reaction period when the nano Ag powder added. The pollutant solution samples were taken at the
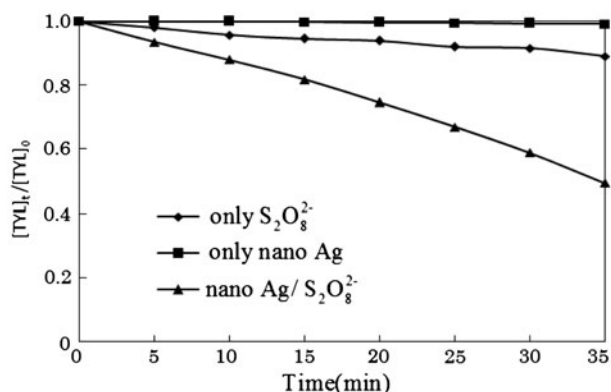

Fig. 3. Effect of UV light on different processes $[TYL]_0 = 50$ mg/L, $[S_2O_8^{2-}]_0 = 100$ mM, pH_0 = natural, $T_0 = 25°C$, [nano Ag]$_0$ = 0.4 g/L.

desired time intervals and were analyzed with a UV/Vis spectrophotometer (Shimadzu UV-160) at $\lambda_{max} = 300$ nm with a calibration curve based on the Beer–Lambert law. The degradation efficiency (X) of TYL antibiotics was obtained at any time, as in following equation [18]:

$$X = \frac{C_t}{C_0} \tag{6}$$

Degradation efficiency was not considerable when using peroxydisulfate alone and nanosilver alone (Fig. 3).

2.2. Analytical method

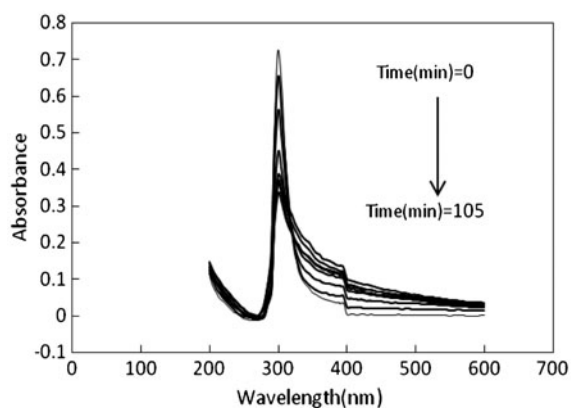The UV–Vis spectra of TYL were recorded from 200 to 800 nm using a UV–Vis spectrophotometer with

Fig. 4. UV–Vis spectra of TYL after different times of nano Ag/$S_2O_8^{2-}$ process $[TYL]_0 = 50$ mg/L, $pH_0 = 6.0$, $[S_2O_8^{2-}]_0 = 100$ mM, [nano Ag]$_0$ = 0.4 g/L, $T = 25°C$.
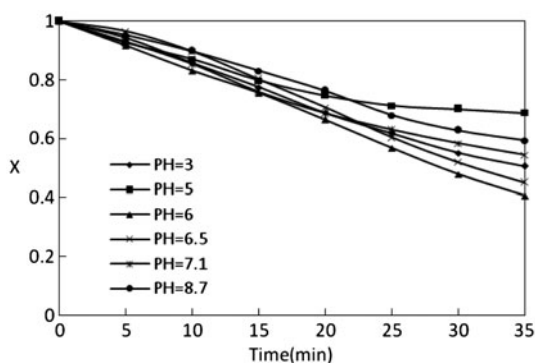
Fig. 5. Effect of pH on the degradation efficiency of the nano $Ag/S_2O_8^{2-}$ process $[TYL]_0 = 50$ mg/L, $T_0 = 25°C$, $[S_2O_8^{2-}]_0 = 100$ mM, [nano Ag]$_0$ = 0.4 g/L.

a spectrometric quartz cell (1 cm path length). The maximum absorbance wavelength (λ_{max}) of TYL can be found at 300 nm from the spectra. Therefore, the concentration of the TYL in the reaction mixture at different reaction ($[TYL]_0 = 50$ mg/L, pH$_0$ = 6.0, $[S_2O_8^{2-}]_0 = 100$ mM, [nano Ag]$_0$ = 0.4 g/L, $T = 25°C$) times were determined by measuring the absorption intensity at $\lambda_{max} = 300$ nm and from a calibration curve. As it is presented in Fig. 4, the absorption band relating to different molecular parts of this substrate, at $\lambda_{max} = 300$ nm, is decreased with respect to time. In this study, the absorbance decrease at 300 nm was measured to follow the degradation of TYL.

3. Result and discussion

3.1. Effect of pH

The effect of initial pH value of solutions on the degradation of TYL by nano $Ag/S_2O_8^{2-}$ process was

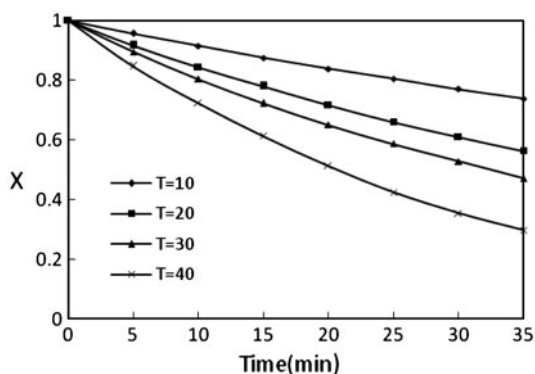studied in the pH range of 3.0–8.7 and the results were shown in Fig. 5. The optimum pH for the highest degradation efficiency of TYL by the nano $Ag/S_2O_8^{2-}$ system was at near neutral value 6.0. The degradation efficiency is drastically decreased when pH increases from 6.0 to 8.7. Generally, from the experimental data, it seems that degradation rate of TYL is significantly faster even in slightly acidic solutions (pH 5–6) as compared to slightly alkaline ones [19]. Under acidic conditions, the breakdown of persulfate into sulfate free radicals can be further acid catalyzed as follows [20]:

$$S_2O_8^{2-} + H^+ \rightarrow HS_2O_8^- \qquad (7)$$

$$HS_2O_8^- \rightarrow SO_4^{2-} + SO_4^{-\cdot} + H^+ \qquad (8)$$
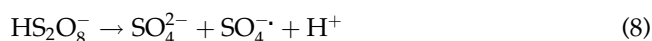
3.2. Effect of temperature

The results presented in Fig. 6 indicate that the degradation efficiency increases when temperature increase from 10 to 40°C after 35 min. The obtained results show with a clear indication that k_{ap} of TYL degradation is significantly affected by reaction temperature and increased with the raise in temperature. The Arrhenius expression, showing the relationship between the reaction temperature and the specific reaction rate, k, is expressed as follows [21]:

$$k = Ae^{-E_a/RT} \qquad (9)$$

where A is preexponential (or frequency) factor; E_a is the activation energy (J mol^{-1}); R is the ideal gas constant (8.314 J mol^{-1} K^{-1}); T is the reaction absolute

Fig. 6. Effect of temperature on the degradation efficiency of the nano $Ag/S_2O_8^{2-}$ process; $[TYL]_0 = 50$ mg/L, pH$_0$ = natural, $[S_2O_8^{2-}] = 100$ mM, [nano Ag]$_0$ = 0.4 g/L.
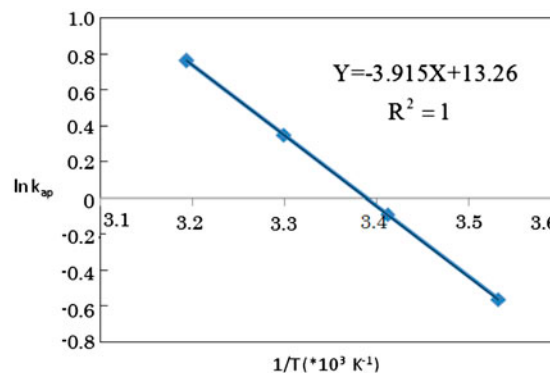
Fig. 7. Plot of ln k_{ap}–(1/T) for the degradation of TYL by nano $Ag/S_2O_8^{2-}$ process; $[TYL]_0 = 50$ mg/L, pH$_0$ = natural, $[S_2O_8^{2-}] = 100$ mM, [nano Ag]$_0$ = 0.4 g/L.
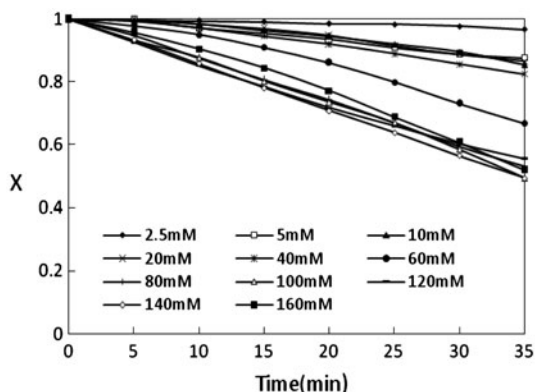
Fig. 8. Effect of persulfate concentration on the degradation efficiency of the nano $Ag/S_2O_8^{2-}$ process; $[TYL]_0 = 50$ mg/L, $pH_0 = $ natural, $T_0 = 25℃$, [nano $Ag]_0 = 0.4$ g/L.

Fig. 9. Effect of nano Ag dosage on the degradation efficiency of the nano $Ag/S_2O_8^{2-}$ process; $[TYL]_0 = 50$ mg/L, $pH_0 = $ natural, $[S_2O_8^{2-}] = 100$ mM, $T = 25℃$.

temperature (K). Due to the narrow temperature range employed in this study (10–40℃), variations of the preexponential factors and the activation energies of the empirical Arrhenius expressions of the reaction of the degradation of TYL may be neglected. The relationships of ln (k_{ap}) vs. $\frac{1}{T}$ are plotted in Fig. 7. Good linear relationships exist between the plots of ln (k_{ap}) and $\frac{1}{T}$ because the regression coefficient was 1.0. Based on the slope $\left(-\frac{E}{R}\right)$ and intercepts (ln A) of the plot in Fig. 8, E and in Arrhenius form (Eq. (9)) are determined i.e. $E = 32.552$ kJ mol^{-1} and $A = 3.06 \times 10^8$ min^{-1}. Therefore, the Arrhenius form of the TYL degradation can be described as:

$$k = 9630.5 \exp\left[-\frac{32.552}{RT}\right] (\text{min}^{-1}) \tag{10}$$

3.3. Effect of $S_2O_8^{2-}$ concentration

The initial concentration of peroxydisulfate was found to be an important parameter for the degradation of TYL in the nano $Ag/S_2O_8^{2-}$ process. The degradation rate of TYL increased with increase in the $S_2O_8^{2-}$ concentration from 2.5 to 100.0 mM. The increase in initial $S_2O_8^{2-}$ concentration leads to a considerable improving effect on the degradation efficiency. This can be due to more sulfate and hydroxyl radical generation (Eqs. (2), (4), and (5)) [22]. Hence, 100.0 mM of peroxydisulfate was chosen as an optimum dose.

3.4. Effect of immobilized nano silver dosage

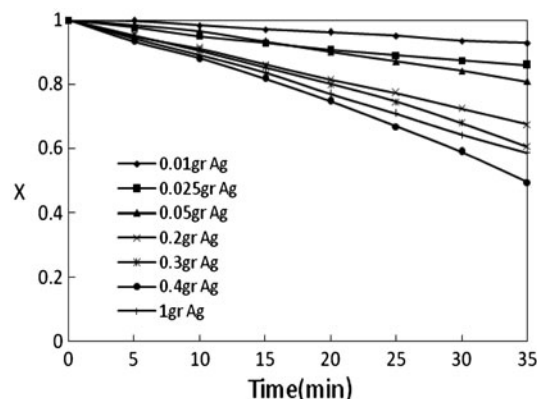The effect of nano Ag concentration on the degradation rate of TYL was studied by varying [nano Ag]$_0$

from 0.01 to 0.4 g/L and at the experiment condition of $[TYL]_0 = 50$ mg/L, $[S_2O_8^{2-}]_0 = 100$ mM, pH = natural, and $T = 25℃$, and the results are presented in Fig. 9. It can be seen that the degradation rate of TYL was almost increased with the increasing of nanosilver dosage. It was reported that Ag was the most efficient metal for the activation of persulfate among 9 transition metals tested by Anipsitakis and Dionysiou [23]. In fact, persulfate oxidation was usually carried out under heat-, photo- or metal ion-catalyzed conditions because the reaction rate could be greatly accelerated. Highly reactive species, such as sulfate radicals ($SO_4^{-\cdot}$) and hydroxyl radicals (HO$^\cdot$), could be quickly generated as a result of decomposition of persulfate ions in aqueous solutions, which were able to oxidize many organic substances into carbon dioxide [24].

3.5. Kinetic study

The kinetics of TYL degradation by nano $Ag/S_2O_8^{2-}$ oxidation process under various reaction conditions ($[TYL]_0 = 50$ mg/L, $pH_0 = $ natural, $[S_2O_8^{2-}] = 100$ mM, [nano $Ag]_0 = 0.4$ g/L) has been investigated. In all the following experiments, mineralization may be described assuming a first-order reaction (Eq. (11)) [21,25,26]:

$$r = -\frac{dC}{dt} = kC^n \tag{11}$$

where r, t, k, and n are the rate of degradation, time, experimental pseudo-first-order reaction rate constant, and order of the reaction, respectively. As it is well known, the rate constant is related to temperature by Arrhenius equation:
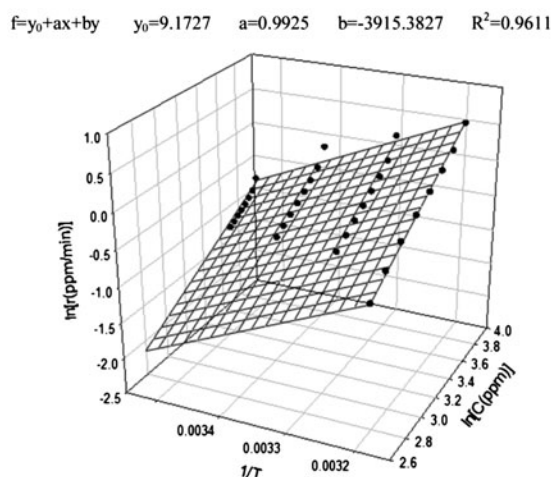
f=y0+ax+by   y0=9.1727   a=0.9925   b=-3915.3827   R²=0.9611

Fig. 10. Correlation diagram for experimental kinetic data; z, x, and y are $\ln r$, $\ln C$, and $\frac{1}{T}$, respectively; [nano Ag]$_0$ = 0.4 g/L, [TYL]$_0$ = 50 ppm, [S$_2$O$_8^{2-}$] = 100 mM, pH 6.0.
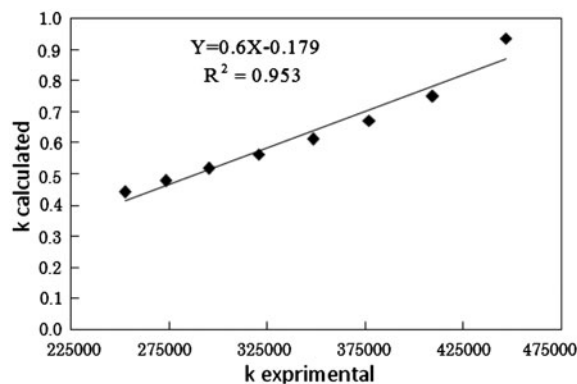

Y=0.6X-0.179
R^2 = 0.953

Fig. 11. Plot of calculated rate constant vs. experimental rate constant for nano Ag/S$_2$O$_8^{2-}$ process.

$$r = 9630.5 \exp\left[-\frac{32.552}{RT}\right] C^{0.9925} \tag{14}$$

$$k = k_0 e^{-E_a/RT} \tag{12}$$

where k_0, E_a, and R are frequency factor, activation energy, and the universal constant of gases, respectively. Substituting Eq. (12) into Eq. (11), one can write the logarithmic form of Eq. (13):

$$\ln r = \ln k_0 - \frac{E_a}{R}\frac{1}{T} + n\ln[C] \tag{13}$$

In Fig. 10, experimental data has been marked with bold dots and the fitted 3D equation with a meshed plane. Variables z, x, and y are attributed to the $\ln r$, $\ln C$, and $\frac{1}{T}$, respectively, and from the coefficients of a, b, and c, kinetic parameters can be obtained. Activation energy and kinetic parameters with the coefficient of determination (R^2) are given in Table 2. As the obtained values of n indicate a pseudo-first-order reaction, rate can be attributed to the degradation of TYL with nano Ag/S$_2$O$_8^{2-}$ process under optimum conditions. Finally degradation rate of TYL is assumed to be pseudo-first-order reaction with respect to TYL concentration, which is expressed as follows:

Table 2
Kinetic parameters of the nano Ag/S$_2$O$_8^{2-}$ process

k_0 (min^{-1})	E_a (kJ/mol)	n	k at 25°C (min^{-1})	R^2
5.78×10^5	32.552	0.9925	1.144	0.9611

The plots of experimentally observed and theoretically calculated rate constant values are shown in Fig. 11. The results from the plot reveal that the proposed kinetic model is well in agreement with the experimental ones. The rate law by this kinetic modeling is theoretically predicted and varies with experimental conditions. But still this model provides the information about the effect of exact operational parameters.

4. Conclusion

In this work, degradation of TYL in aqueous solution by persulfate in the presence of immobilized nanosilver was investigated. The results showed that the degradation efficiency of TYL by persulfate was significantly influenced by pH, persulfate concentration, temperature, and nano Ag dosage. A suitable operating condition was selected as: [nano Ag]$_0$ = 0.4 g/L, [TYL]$_0$ = 50 ppm, [S$_2$O$_8^{2-}$] = 100 mM, pH = 6.0, and temperature at 40°C. The kinetics study indicated that the degradation kinetics of TYL followed the pseudo-first-order kinetics. The rate of TYL degradation was: (1) increased with the increase in pH in the range of 3.0–6.0 and then, decreased with the continuous increase of pH in the range of 6.0–8.7; (2) increased with the increase in initial concentration of S$_2$O$_8^{2-}$ in the range of 2.5–100 mM and then, slightly decreased with the further raise in S$_2$O$_8^{2-}$ concentration in the range of 100–160 mM; (3) increased with the increase of nano Ag dosage in the range of 0.01–0.40 g/L; (4) also increased with the increase in

temperature. Based on the rate constants obtained at different temperatures, the empirical Arrhenius expression of TYL degradation was derived. The derived activation energy for TYL degradation by nano $Ag/S_2O_8^{2-}$ oxidation is 32.552 kJ mol^{-1}.

References

[1] N. Prado, J. Ochoa, A. Amrane, Biodegradation and biosorption of tetracycline and tylosin antibiotics in activated sludge system, Process Biochem. 44 (2009) 1302–1306.

[2] A.J. Watkinson, E.J. Murby, S.D. Costanzo, Removal of antibiotics in conventional and advanced wastewater treatment: Implications for environmental discharge and wastewater recycling, Water Res. 41 (2007) 4164–4176.

[3] E.S. Elmolla, M. Chaudhuri, Degradation of amoxicillin, ampicillin and cloxacillin antibiotics in aqueous solution by the UV/ZnO photocatalytic process, J. Hazard. Mater. 173 (2010) 445–449.

[4] J. Paesen, W. Cypers, K. Pauwels, E. Roets, J. Hoogmartens, Study of the stability of tylosin A in aqueous solutions, J. Pharm. Biomed. Anal. 13 (1995) 1153–1159.

[5] J.S. Teeter, R.D. Meyerhoff, Aerobic degradation of tylosin in cattle, chicken, and swine excreta, Environ. Res. 93 (2003) 45–51.

[6] I.R. Bautitz, R.F. Pupo Nogueira, Degradation of tetracycline by photo-fenton process-solar irradiation and matrix effects, J. Photochem. Photobiol. A 187 (2007) 33–39.

[7] A. Karimi, F. Mahdizadeh, M.R. Eskandarian, Enzymatic in situ generation of H_2O_2 for decolorization of acid blue 113 by fenton process, Chem. Ind. Chem. Eng. Q. 18 (2012) 89–94.

[8] M.R. Eskandarian, F. Mahdizadeh, L. Ghalamchi, S. Naghavi, Bio-fenton process for acid blue 113 textile azo dye decolorization: Characteristics and neural network modeling, Desalin. Water Treat. 22 (2013) 1–9.

[9] F. Mahdizadeh, M. Eskandarian, J. Zabarjadi, A. Ehsani, A. Afshar, Silver recovery from radiographic film processing effluents by hydrogen peroxide: Modeling and optimization using response surface methodology, Korean J. Chem. Eng. 31 (2014) 74–80.

[10] M.R. Eskandarian, A. Karimi, M.R. Shabgard, Studies on enzymatic biomachining of copper by glucose oxidase, J. Taiwan Inst. Chem. Eng. 44 (2013) 331–335.

[11] M. Klavarioti, D. Mantzavinos, D. Kassinos, Removal of residual pharmaceuticals from aqueous systems by advanced oxidation processes, Environ. Int. 35 (2009) 402–417.

[12] B.K. Dutta, S. Harimurti, S. Chakrabarti, D. Vione, Degradation of diethanolamine by Fenton's reagent combined with biological post-treatment, Desalin. Water Treat. 19 (2010) 286–293.

[13] L.G. Devi, S.G. Kumar, K.M. Reddy, C. Munikrishnappa, Effect of various inorganic anions on the degradation of congo red, a di azo dye, by the photo-assisted fenton process using zero-valent metallic iron as a catalyst, Desalin. Water Treat. 4 (2009) 294–305.

[14] J. Feng, X. Hu, P.L. Yue, H.Y. Zhu, G.Q. Lu, Discoloration and mineralization of reactive red HE-3B by heterogeneous photo-Fenton reaction, Water Res. 37 (2003) 3776–3784.

[15] J.H. Sun, S.P. Sun, M.H. Fan, H.Q. Guo, L.P. Qiao, R.X. Sun, A kinetic study on the degradation of p-nitroaniline by fenton oxidation process, J. Hazard. Mater. 148 (2007) 172–177.

[16] R. Andreozzi, V. Caprio, A. Insola, R. Marotta, Advanced oxidation processes (AOP) for water purification and recovery, Catal. Today 53 (1999) 51–59.

[17] Y. Deng, C.M. Ezyske, Sulfate radical-advanced oxidation process (SR-AOP) for simultaneous removal of refractory organic contaminants and ammonia in landfill leachate, Water Res. 45 (2011) 6189–6194.

[18] M.H. Rasoulifard, S.M.M. Doust Mohammadi, A. Heidari, E. Farhangnia, Degradation of acid red 14 by silver ion-catalyzed peroxydisulfate oxidation in an aqueous solution, Turkish J. Eng. Environ. Sci. 35 (2011) 1–8.

[19] K. Ntampegliotis, A. Riga, V. Karayannis, V. Bontozoglou, G. Papapolymerou, Decolorization kinetics of procion H-exl dyes from textile dyeing using fenton-like reactions, J. Hazard. Mater. 136 (2006) 75–84.

[20] C. Liang, Z.S. Wang, C.J. Bruell, Influence of pH on persulfate oxidation of TCE at ambient temperatures, Chemosphere 66 (2007) 106–113.

[21] J. Saien, A.R. Soleymani, J.H. Sun, Parametric optimization of individual and hybridized AOPs of Fe^{2+}/H_2O_2 and $UV/S_2O_8^{2-}$ for rapid dye destruction in aqueous media, Desalination 279 (2011) 298–305.

[22] J.H. Sun, S.P. Sun, M.H. Fan, H.Q. Guo, L.P. Qiao, R.X. Sun, A kinetic study on the degradation of p-nitroaniline by Fenton oxidation process, J. Hazard. Mater. 148 (2007) 172–177.

[23] G.P. Anipsitakis, D.D. Dionysiou, Transition metal/UV-based advanced oxidation technologies for water decontamination, Appl. Catal. B, Environ. 54 (2004) 155–163.

[24] S.X. Li, D. Wei, N.K. Mak, Z.W. Cai, X.R. Xu, H.B. Li, Y. Jiang, Degradation of diphenylamine by persulfate: Performance optimization, kinetics and mechanism, J. Hazard. Mater. 164 (2009) 26–31.

[25] S.P. Sun, C.J. Lie, J.H. Sun, S.H. Shi, M.H. Fan, Q. Zhou, Decolorization of an azo dye orange G in aqueous solution by Fenton oxidation process: Effect of system parameters and kinetic study, J. Hazard. Mater. 161 (2009) 1052–1057.

[26] N. Kang, D.S. Lee, J. Yoon, Kinetic modeling of fenton oxidation of phenol and monochlorophenols, Chemosphere 47 (2002) 915–924.